Applied Catalysis B: Environmental 180 (2016) 362–371

Contents lists available at ScienceDirect

Applied Catalysis B: Environmental

journal homepage: www.elsevier.com/locate/apcatb

Photocatalytic properties of titania thin films prepared by sputtering versus evaporation and aging of induced oxygen vacancy defects

Bodo Henkel[a], Thomas Neubert[b], Sebastian Zabel[a], Constanze Lamprecht[c], Christine Selhuber-Unkel[c], Klaus Rätzke[a], Thomas Strunskus[a], Michael Vergöhl[b], Franz Faupel[a,*]

[a] Institute for Materials Science, Chair for Multicomponent Materials, Faculty of Engineering, Christian-Albrechts-University of Kiel, Kaiserstraße 2, D-24143 Kiel, Germany
[b] Fraunhofer Institute for Surface Engineering and Thin Films (IST), Bienroder Weg 54 E, 38108 Braunschweig, Germany
[c] Institute for Materials Science, Biocompatible Nanomaterials, Faculty of Engineering, Christian-Albrechts-University of Kiel, Kaiserstraße 2, D-24143 Kiel, Germany

ARTICLE INFO

Article history:
Received 13 April 2015
Received in revised form 17 June 2015
Accepted 19 June 2015
Available online 25 June 2015

Keywords:
TiO2
Photocatalysis
Sputtering
Evaporation
Aging
Oxygen vacancy defects
Methylene blue

ABSTRACT

In order to understand the variations in photocatalytic efficiencies of titania thin films prepared by different physical vapor deposition techniques, we studied the microstructure and resulting properties for the two widely used PVD methods, electron beam evaporation and reactive pulsed DC magnetron sputtering. In addition, we investigated the effect of oxygen vacancy defects induced by tempering in reducing atmospheres and the aging behavior. After deposition, several tempering series in oxygen, air, argon, and forming gas were carried out to control the amount of oxygen vacancy defects. The films were characterized with respect to crystallinity, texture, grain growth, grain structure, surface roughness, light transmission as well as band gap energy; the photocatalytic efficiency was measured via methylene blue degradation. The results show different nucleation and growth mechanisms between evaporated and sputtered titania thin films, resulting in severe influence on photocatalytic efficiency. The evaporated thin films exhibited homogeneous nucleation and growth, and stayed in the anatase structure even after tempering at 800 °C for 1 h. In contrast, the sputtered thin films started to form grains at the interface to the substrate and showed heterogeneous nucleation and growth. Moreover, the sputtered films already formed rutile when tempered at 600 °C for 1 h. The gain in surface area due to tempering, which promotes adsorption of photocatalytic reactants, was more pronounced in sputtered thin films (+29%) compared to evaporated thin films (+6%). Films with oxygen vacancy defects, preserved by tempering in argon or induced by tempering in forming gas, showed a large improvement in photocatalytic efficiency. However, aging of the samples over a period of 19 months lead to a progressive decline in efficiency, finally reaching the level of thin films tempered in air, which had remained stable over the same 19 month period. This strongly questions widely applied concepts based on improving the photocatalytic efficiency via oxygen vacancy defects.

1. Introduction

Photocatalysis is an interesting field of research and application with the promise to use readily available solar power for air and water purification. Following the first publication that promoted TiO_2, titania, as a photocatalyst in 1938 [1], the field became very active in the 1970s induced by the research of Akira Fujishima [2]. Nowadays, climate change is a major issue and it is more important than ever to harvest solar power and find economical ways to purify water for countries in need of clean drinking water.

Although photocatalysis is only one word, it is an interdependent combination of several physical and chemical mechanisms. The catalyst is a solid semiconductor with a suitable band gap for a particular application and light source, and to surpass the required redox potentials for the chemical reactions. On the one hand, you want to absorb as many photons as possible. This calls for a smaller band gap in the case of sunlight. For artificial light sources, such as LEDs, the requirements for the semiconductor band gap will

* Corresponding author. Fax: +49 431 880 6229.
E-mail address: ff@tf.uni-kiel.de (F. Faupel).

http://dx.doi.org/10.1016/j.apcatb.2015.06.041
0926-3373/

depend on the specific radiation characteristics of the light source, and here a rather specific band gap may be suitable. On the other hand, you want to generate charge carriers with sufficient redox potential to enable the desired chemical reactions on the surface of the photocatalyst, which would call for a band gap as wide as possible. Thus, the ideal properties of the photocatalyst will depend on the light source and the particular application. When irradiated with light of sufficient wavelength, photons will be absorbed and charge carrier pairs generated. These will make a random walk through the bulk and either recombine or reach the thin film's surface. In the present paper, the interaction substance is deionized water with the organic dye Methylene Blue as a contaminant. The dye molecules adsorb at the thin film's surface and available charge carriers can transfer from the catalyst to the molecules and induce chemical reactions, which degrade the dye. The three main processes (charge carrier generation, diffusion to the surface, and reactant diffusion) influence the photocatalytic efficiency and are determined by materials properties.

The choice of semiconductor determines the band structure and band gap. Light absorption and charge carrier generation are more likely to happen in a direct band gap compared to an indirect one, but the same holds for recombination [3]. While smaller band gaps are desirable for long wavelength, bigger band gaps offer the advantage of a greater reduction potential [4,5]. TiO_2 is a wide band gap semiconductor with an indirect band gap of 3.26 eV for the anatase phase and a direct band gap of 3.05 eV for the rutile phase [4]. Anatase is the most commonly used crystal phase, because it shows the highest overall photocatalytic efficiency. Rutile is undesirable in most cases, as it dramatically decreases the catalyst's efficiency [4,6,7]. Only a small, favorable, synergetic regime in the combination of the two phases is reported in literature [8], but is controversial [7].

Another highly important property is crystallinity, which influences band gap energy and charge carrier lifetime [3,7,9]. Grain size increases during crystallization and influences the band gap, because of quantum confinement [10]. However, for photocatalysis, grain boundaries are far more interesting since they are the most active recombination sites, and therefore hinder charge carriers from reaching the surface [7].

The catalyst surface area is important, as the chemical reaction only happens at the surface where the charge can be transferred [9,11]. Additionally, hydroxyl groups are bound to the surface and known to promote photocatalysis [4,12]. The location and amount of oxygen vacancies are of great importance. If distributed throughout the bulk, there is a red shift of the band gap, enabling the catalyst to effectively absorb sunlight [12,13]. If oxygen vacancies are limited to the surface, better charge separation [14] and higher reactivity with the adsorbing molecules are achieved, resulting in higher photocatalytic efficiency [15]. Bulk oxygen vacancies are not stable, if the surface defects are not saturated, and – the other way round – photocatalytic efficiency in UV-A regime is considerably reduced by additional oxygen vacancy defects in the bulk [16].

Among possible candidates, TiO_2 is highly interesting for photocatalytic applications: it has the most efficient photoactivity, its band gap matches many important redox potentials, it is chemically stable and mechanically robust, cheap, and is considered safe for humans and the environment [4,12,17–19].

Several methods of producing titania thin films have been investigated presently [4,12,20]. A popular method is sol-gel due to its simplicity and the possibility of low cost batch processing. Nevertheless, physical vapor deposition (PVD) techniques are of growing interest for producing photocatalytically active thin films, because they are not limited to deposition in thermodynamic equilibrium.

The exact reasons for differences in photocatalytic efficiencies between different PVD techniques are not fully understood. We present a detailed comparative study in photocatalysis of two PVD methods, which are well established and already used for other purposes in industry.

2. Experimental

2.1. Deposition of titania thin films

For both deposition methods, polished quartz glass ($1 \times 1\,cm^2$, QSIL GmbH) and phosphor doped Si wafer pieces (1 0 0) with native oxide ($1 \times 1\,cm^2$ and $0.5 \times 0.5\,cm^2$, Goodfellow GmbH) were used as substrates. Although the substrates are seemingly different, the growth of TiO_2 during deposition always started on a substrate layer of amorphous SiO_2.

Electron beam evaporation was done inside Pfeiffer-Balzers PLS 570 with a TFI Telemark Model 261 Multi-Pocket Electron Beam Gun. The chamber was evacuated to a pressure of 10^{-5} Pa prior to each deposition. An initial layer of about 10 nm SiO (99.8%) at a deposition rate of 6 nm/min was deposited with a thermal evaporator. Afterwards, approximately 140 nm SiO_2 (99.9%) at a deposition rate of 6.0 nm/min was deposited with the electron beam gun at an oxygen flow rate of 20 sccm, leading to a process pressure of 10^{-2} Pa. On top of that, 425 nm Ti_3O_5 (99.99%) at a deposition rate of 6.0 nm/min was deposited with the electron beam gun with an oxygen flow of 20 sccm, leading to a process pressure of 10^{-2} Pa. All depositions by evaporation were performed at room temperature.

Sputtering was done with a self-made vacuum deposition chamber built out of commercially available components. With this chamber we performed unipolar, reactive, pulsed DC magnetron sputtering. A rotary pump (Agilent Technologies, SH-110) in combination with a turbo molecular pump (Pfeiffer Vacuum, HiPace 400) was used. The Ti target (Goodfellow, 99.99%, 5 cm diameter) was attached to a DC planar magnetron source (Thin Film Consulting, ION'X-2UHV). The DC power was pulsed to discharge the target and therefore reduce the oxidation of the target trench and thus keep sputter rates high, even at high oxygen flow rates. To pulse the plasma, a self-made pulsing-box with a high power MOSFET (Behlke Power Electronics, HTS 31CF I) was triggered by a frequency generator (PeakTech, DDS Function Generator 4025). The trigger signal was rectangular with 5 V peak-to-peak amplitude, 0 V minimum, 50 kHz frequency, and 55% duty cycle. In this regime the switched power output reaching the magnetron was of feasible near-rectangular shape with a very short overshoot at the beginning of duty on phases, checked with a digital oscilloscope (Agilent Technologies, DSO 1002A) with high voltage probe (Agilent Technologies, 10.076B). The switched power generated by the power source (Advanced Energy, MDX 500) was 90 W ($28.3\,W/cm^2$) on average. For the process gases, a flow rate controller (MKS, Multi Gas Controller 647C) was used to control two flow regulators, one for argon (MKS, 1179B) and the other for oxygen (MKS, MF1 L01321CMAV0).

The initial pressure before each sputtering experiment was below 5×10^{-4} Pa. Before each deposition, oxygen was removed from the target by plasma (250 sccm Ar, 2.7 Pa) for 10 min. Afterwards, oxygen (2.5 sccm, 2.8 Pa) was injected. After a stabilizing phase of 5 min, shutters were opened for deposition at a rate of 19 nm/min. The distance between target and sample was 41 mm with an angle of incidence of 50°. The sample stage rotated at 10 rpm to assure homogeneous films on all substrates. The film thicknesses were 426 ± 7 nm. Because the sample holder was on floating potential, a self-bias of ca. 26 V peak and 13 V average was measured. All sputter depositions were performed at room temperature, but nevertheless, the samples were heated due to atom and ion bombardment. The temperature of the sample holder plate below the sample was measured to be around 60 °C at the end of the sputtering process. From the measured temperature increase

beneath the sample holder plate and the specific setup, the sample surface temperature is estimated to be 200 °C.

2.2. Tempering of titania thin films

Both sputtered and evaporated thin films were tempered after deposition according to different parameter series in an oven (GERO SR 70–500/12). The temperature was varied (400–800 °C) while the time at temperature (TAT) was kept constant at 1 hour in air. In a second series at 600 °C in air, TAT was varied (5, 10, 30, 60, 120 min). In a third series, the atmosphere was varied (oxygen, air, argon, and forming gas (95% N_2 + 5% H_2)), with TAT of 1 h and 600 °C temperature. One sample was kept at room temperature (RT) in air and used as a control.

2.3. Characterization

Crystallinity, texture and the occurrence of TiO_2 polymorphs were measured by X-ray diffraction (XRD; Seifert XRD 3000, using Cu Kα) and confocal Raman spectroscopy (WITec, alpha300AR). Expected possible TiO_2 polymorphs for the experiment are anatase and rutile. Surface topography was imaged by atomic force microscopy (AFM) (JPK, NanoWizard 3) operated in AC mode using ACTA-cantilevers (spring constant ~40 N/m, resonance frequency ~300 kHz; Applied NanoStructures, Inc., Mountain View, USA). Image processing and analysis (surface roughness and surface area) of AFM data were carried out with the software Gwyddion version 2.37 (Gwyddion – Free SPM, sourceforge.net). Optical properties were measured by UV–vis spectroscopy (PerkinElmer Lambda 900 UV–vis/NIR spectrophotometer). UV–vis data were used to evaluate band gap energies [21,22]. $\sqrt{\alpha h\nu}$ was plotted vs. photon energy to show the indirect band gap's energy, with α being the absorption coefficient, h the Planck constant and ν the light's frequency. Linearly extrapolating the absorption edge to the abscissa gives the band gap energy. Assuming a direct band gap, an analogue evaluation was performed by plotting $(\alpha h\nu)^2$ over photon energy. An exemplary fit is shown as inset in Fig. 4 in Section 3. The error bars are deduced by testing both worst cases of a barely matching fit, for each measurement. Film thicknesses and derived deposition rates were determined by measuring film steps on partially covered samples using a surface profilometer (Bruker, DektakXT). The measured film thicknesses were cross-checked by ellipsometry measurement (Sentech SE 850) and with scanning electron microscopy (SEM; Zeiss Supra 55VP) of cross-sections. Ellipsometry was also used to determine the refractive index. SEM was used to make top view and cross-sectional measurements to determine thin film structure, grain size and shape. The efficiency of photocatalytic degradation of molecules was measured with a self-made reactor with a methylene blue solution (MB) as an organic test substance. The reactor is built in accordance to ISO 10678 / DIN 52980 with the additional capability to measure smaller samples [23,24]. Methylene blue powder (Sigma–Aldrich, CAS 7220-79-3) was dissolved in deionized water to a concentration of $c_0 = (10 \pm 0.5)$ μmol/l. An aliquot of 6.5 ml of MB solution was pipetted into a quartz cuvette, and the sample, fixed to a Teflon® holder, was completely submerged in the solution. The solution was stirred during measurement with a magnetic stirrer. The cuvette was placed in a light-shielded reactor, where only the sample area was irradiated by the UV-LED (Laser Components GmbH, OTLH-0480-UV). The UV-LED was characterized to have its peak wavelength at 369 nm, with an LED specific narrow peak width of 20 nm. Irradiance at the sample position was measured to be stable at (4.77 ± 0.01) mW/cm^2. The solution temperature was monitored to be at room temperature during the whole measurement. The MB concentration of the solution was measured in-situ once every minute by UV–vis spectroscopy (StellarNet EPP2000C-SR-50 with SL5-DH light source). It was assured by measurement that the light of the UV-LED does not reach the UV–vis detector. In the linear measurement regime of a UV–vis device, absorbance is proportional to the concentration of the solute, which was the case for these experiments. Furthermore, it was checked that the UV–vis light itself has no measurable effect on the degradation of MB. Error bars of the MB degradation measurements are typically 2–3% relative error of the respective value, with a minimum error at very low degradation rates. This was determined by evaluating reproducibility experiments with two principally different batches consisting each of several samples of the same type.

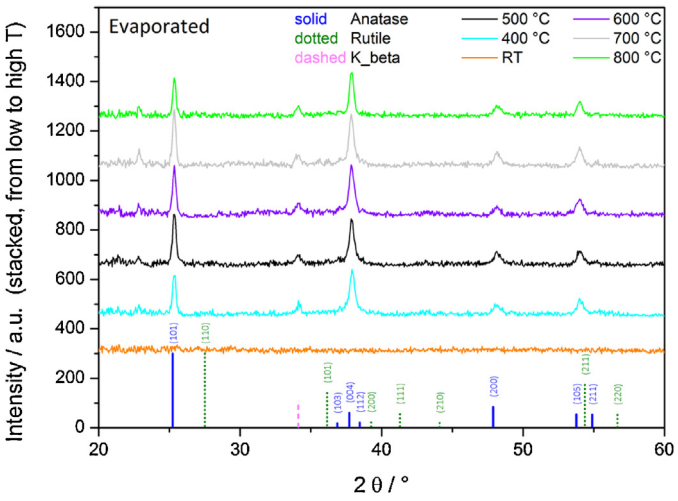

Fig. 1. XRD of temperature series of evaporated TiO_2 thin films (data is stacked for sake of clarity, low temperature at the bottom, high temperature at the top).

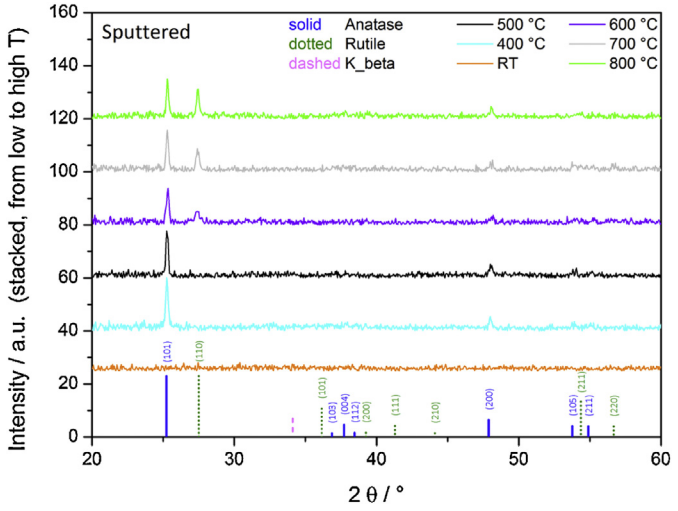

Fig. 2. XRD of temperature series of sputtered TiO_2 thin films (data is stacked for sake of clarity, low temperature at the bottom, high temperature at the top).

3. Results and discussion

3.1. Crystallinity and TiO_2 phases

After tempering, thin films were analyzed by XRD to check for differences in crystallinity and phase composition (Fig. 1 and Fig. 2). In both thin film series, evaporated and sputtered, the untempered thin films are X-ray amorphous, as expected. Already after 1 h at 400 °C, both thin film types show pronounced crystalline peaks identified as anatase phase. They differ, however, in the temper-

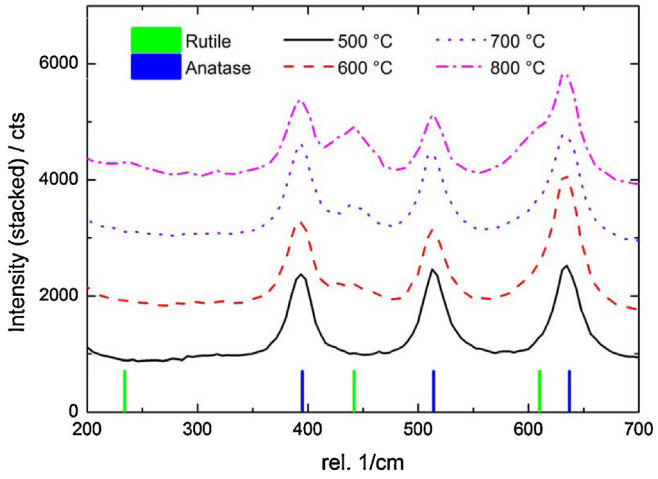

Fig. 3. Raman spectroscopy measurement of sputtered temperature series. TAT was 1 h each (data is stacked for sake of clarity, low temperature at the bottom, high temperature at the top).

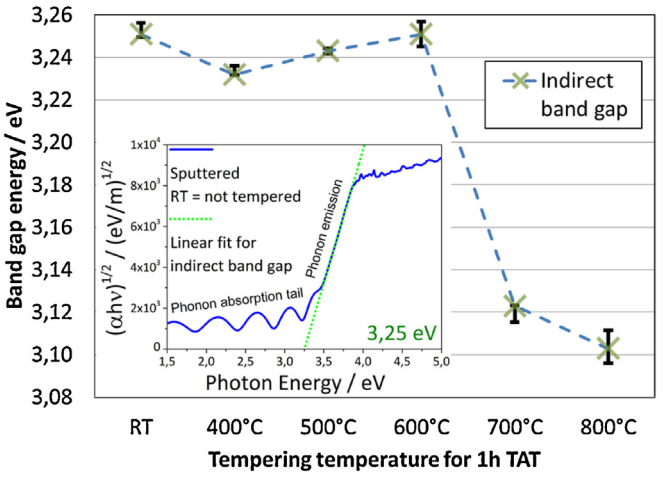

Fig. 4. Band gap energies for temperature series of sputtered thin films, evaluated from UV–Vis measurements. The inset shows exemplary the evaluation method for the indirect band gap. The error bars are determined by testing the range of possible fits by the used method for each measurement.

ature at which the rutile phase is formed. Whereas the evaporated thin films remained completely anatase, even up to 800 °C at 1 h TAT, rutile is visible in XRD for sputtered thin films already at 600 °C with 1 h TAT. Starting temperatures for rutile formation vary among different literature sources in a broad range between 465 °C in [25] and 900 °C in [26]. This pronounced difference in phase formation of evaporated and sputtered thin films indicates once again the strong dependence on details, such as fine structure, type of crystallization and kinetics during deposition. These will be discussed in detail in Section 3.5 "Thin film structure and crystallization".

Aside from phase transformation, texture is an important aspect for photocatalysis, because the crystal planes at the surface – often referred to as facets – are known to have significantly different photocatalytic efficiencies [27–29]. While the sputtered thin films show the typical anatase peak distribution of a powder sample matching nicely the reference, the evaporated thin films have distinct texture. The (0 0 1) plane, visible by the (0 0 4) diffraction, shows about the same intensity as the (1 0 1) plane, which is normally the most prominent. Another distinctive plane is (1 0 5). Both facets {0 0 1} and {1 0 5} are reported to be more reactive than {1 0 1} in literature, with {0 0 1} proving to be the most reactive facets due to their high surface energy, which leads to efficient oxidation of contaminant species [27,30,31]. In contrast {1 0 1} facets have such low surface energy that reduction preferably happens there. Therefore a coexistence of both facet types at the catalyst's surface is synergistically enhancing photocatalysis, because both reactions are necessary in the chemical pathways of degradation [27]. Adding up to this synergy, charge carrier separation is promoted due to the different surface energies and trap states of the facets and hence lowering recombination [32]. The favorable texture of the evaporated thin films should significantly improve their photocatalytic performance compared to the sputtered films. This is indeed reflected partially in the later shown methylene blue degradation results.

XRD measurements for TAT series (data not presented) show principally the same result, also with regard to texture. Significant anatase peaks are already visible in the diffractogram after 5 min at 600 °C, and after 10 min the intensities of characteristic reflections are already the same as after 1 h. Ellipsometry measurements on both thin film types show an increasing refractive index for thin films treated with higher temperatures and longer TAT. This is to be expected; the increase in crystallinity leads to higher density of the thin film, and therefore to a higher refractive index.

Raman spectroscopy measurements of the temperature series of sputtered thin films (Fig. 3) show in detail increasing rutile formation with increasing temperature. The rutile peak at 442 rcm^{-1} is most obvious. The rutile peak at 610 rcm^{-1} partially overlaps with the anatase peak at 637 rcm^{-1}. This leads to the growth of a double peak, which is clearly visible at 800 °C. The rutile peak at 234 rcm^{-1} is naturally quite small and only visible when comparing the graphs. The 500 °C thin film does not contain any measureable rutile. It starts to form in the 600 °C thin film and grows more and more with higher temperatures, shown up to 800 °C. The difference between evaporated and sputtered thin films in forming rutile is an important point, because rutile generally has – despite a small composition window for which positive synergy is reported [8] – a strong negative impact on photocatalytic efficiency [4,6,7].

3.2. Optical properties

In Fig. 4, band gap energies of the temperature series of sputtered thin films are shown, which were evaluated from UV–vis spectra as described in the Section 2 (Fig. 4 inset depicts an example). The band gap stays about the same up to 600 °C 1 h TAT and is in good agreement with literature values of anatase (3.26 eV) [4]. At higher temperatures it decreases to much lower values. Rutile has a lower band gap energy, 3.05 eV, than anatase [4]. Thus, the results support the formation of rutile in the sputtered thin films at higher temperature in agreement with the results in the previous section.

Aside from the rutile influence, in both series of different temperatures and TAT, the evaporated thin films had consistently higher band gap energies than the corresponding sputtered thin films, with a difference ranging between +0.05 and +0.10 eV. This could perhaps be explained by a larger amount of point defects in the sputtered thin films that would decrease the band gap energy by introducing additional energy states inside the anatase band gap [3]. This could be an interesting indicator, because a larger amount of point defects might be another reason for rutile formation in the sputtered thin films in contrast to evaporated ones. Rutile is known to form preferably at defect sites [33].

For light absorption and charge carrier generation, it is preferable to have the lower band gap energy of the sputtered thin films, as described above, because longer wavelengths of the UV-A irradiation can be used for photocatalysis.

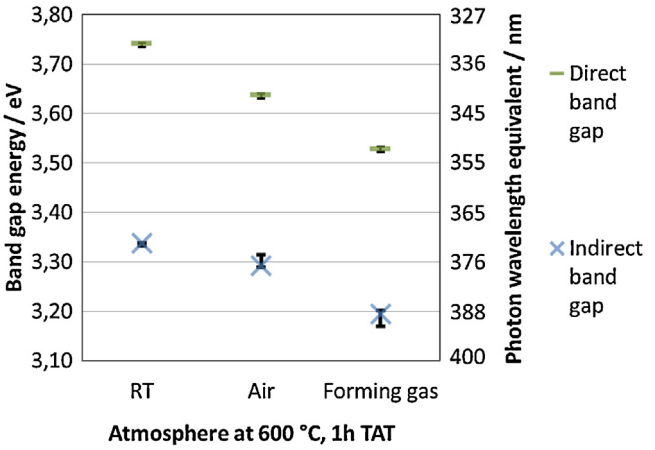

Fig. 5. Band gap energies of tempering atmosphere series of evaporated thin films, evaluated from UV–Vis measurements.

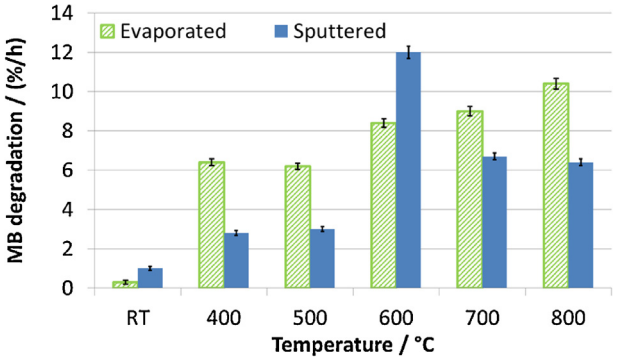

Fig. 6. Methylene blue degradation of temperature series.

In Fig. 5, the band gap energies are compared for evaporated thin films tempered under forming gas atmosphere, tempered in air and untempered (RT). The decrease in band gap energy by tempering under air atmosphere is attributed to a reduced quantum confinement effect, which is only dominant for a range of grain sizes of a few nanometers, reportedly up to 10 nm [18]. Because of that, grain growth by tempering lets the thin film's band gap energy approach the value of bulk anatase. Interestingly, there is an even stronger decrease in band gap energy for the thin films tempered under forming gas atmosphere. We propose that this is due to oxygen vacancy defects induced by the forming gas. These defects would introduce additional states in the anatase band gap [3]. In case of only a small amount of these defects, only localized states would be created. But if there are enough oxygen vacancy defects, the result would be a red shift of the band gap, as reported for bulk oxygen vacancy defects [12,13]. Such a situation would be favorable for photocatalysis, as a larger spectral range could be harvested. However, since we were using UV-A light instead of white light (sunlight), also the direct band gap matching a wavelength of 352 nm, potentially contributes to charge carrier generation. If a commonly used mercury-vapor lamp was used, the positive effect of forming gas would be even higher than already reported in the later section about tempering atmospheres.

3.3. Methylene blue degradation efficiencies

Photocatalytic measurements by degradation of methylene blue as presented in Fig. 6 show pronounced differences between thin film types. When untempered, both series of samples have nearly no photocatalytic degradation (≤1%/h), as expected. The efficiency

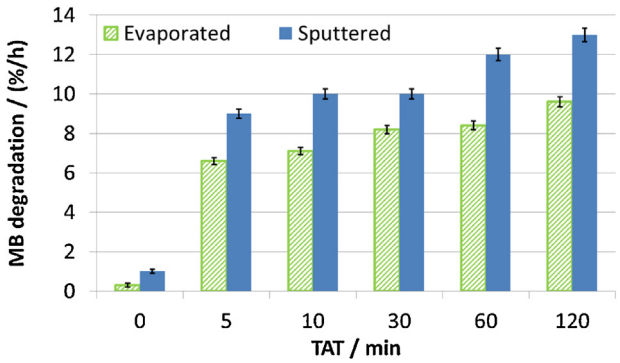

Fig. 7. Methylene blue degradation of TAT series.

of degradation by evaporated thin films significantly increases at 400 °C and continues to improve up to 800 °C. Sputtered thin films, on the other hand, show only a slight increase at 400 °C, and even at 500 °C. Their significant increase in efficiency is at 600 °C, which is also the maximum. After that, it decreases. Sputtered thin films seem to have an improved maximum efficiency. This is astonishing due to the more favorable texture of the evaporated thin films. One reason could be the better UV absorption seen in UV–vis measurements. Another reason could be an increased surface area, which will be addressed in the discussion of the AFM results. The continuous increase of efficiency for evaporated thin films is attributed to their increasing crystallinity with complete absence of rutile, even after treatment at 800 °C. The continuously higher light absorption due to decreasing band gap energy increases efficiency by supplying more charge carriers for the reaction. The maximum in the efficiency found for sputtered thin films is attributed to the formation of rutile at higher temperatures, as shown with XRD and Raman spectroscopy. At 600 °C, where rutile first forms, advantages of good crystallinity, UV absorption and surface structure seem to overcompensate for the disadvantageous rutile. It is likely that without rutile at 600 °C, this maximum would be even more pronounced and then indeed be significantly better than the evaporated counterpart. One possibility to suppress rutile up to higher temperatures would be to sputter with parameters that build fewer defects into the thin film. As shown in [12,33], growth of rutile is promoted at defect sites. Structural reasons for the late increase in efficiency of sputtered thin films will be suggested during discussion of SEM measurements.

Methylene blue degradation results for TAT series presented in Fig. 7 are quite similar to the temperature series of evaporated thin films. Again, there is a very low efficiency for untempered thin films, a pronounced increase at first tempering and a continuous increase after that. As 600 °C is the temperature at which sputtered thin films have their efficiency step in the temperature series, it seems plausible that in TAT results made with this sufficient temperature, there would be no delay of the step in comparison to evaporated thin films. Raman spectroscopy of the sputtered TAT 120 min thin films did not show any increase in rutile compared to the 60 min thin films. Therefore, the degradation can further increase due to larger grains and larger surface area, as will be discussed on the basis of AFM measurements in the next section. For all TATs, sputtered thin films perform better than the evaporated counterparts, i.e. (+233, 36, 41, 22, 43, 35) % better at (RT, 5, 10, 30, 60, 120) min respectively.

3.4. Surface area for molecule adsorption

AFM measurements were performed to resolve surface structure and enable calculation of surface area in order to compare the size of adsorption surface for reactants. This is possible because of three reasons. First, the resolution of these measurements is so

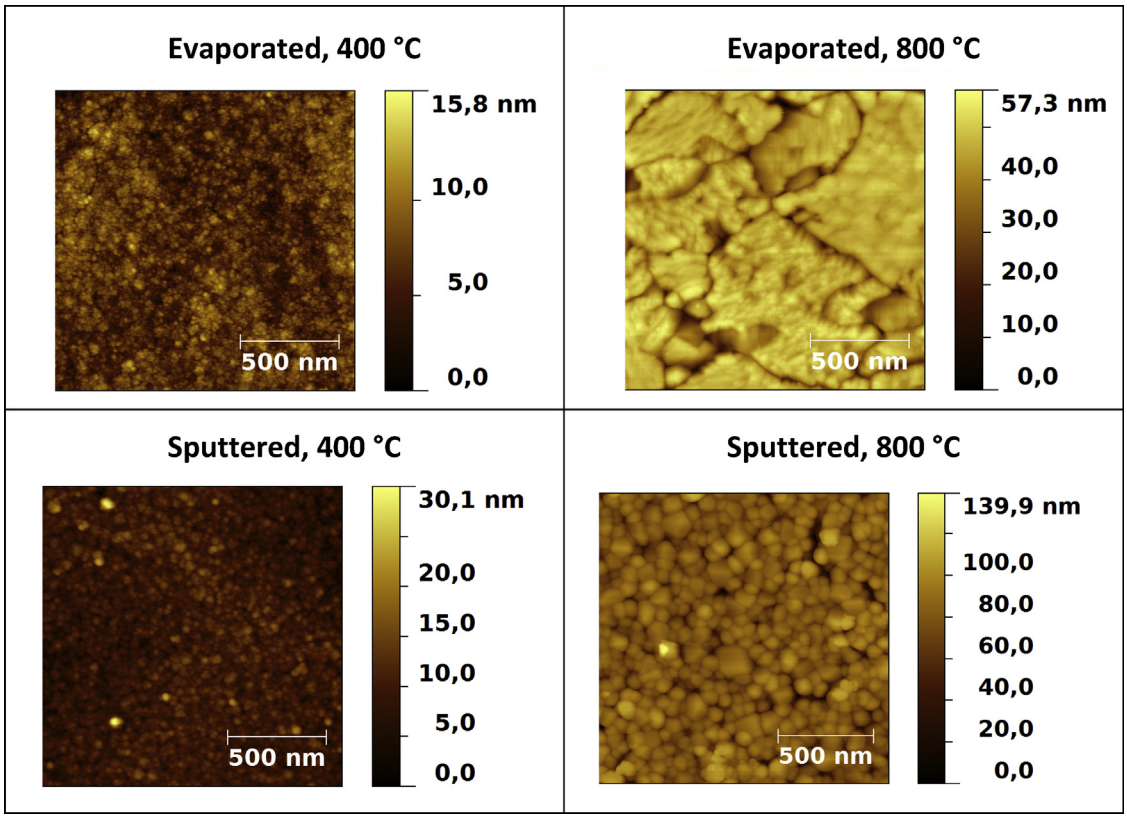

Fig. 8. AFM of temperature series, TAT 1 h each.

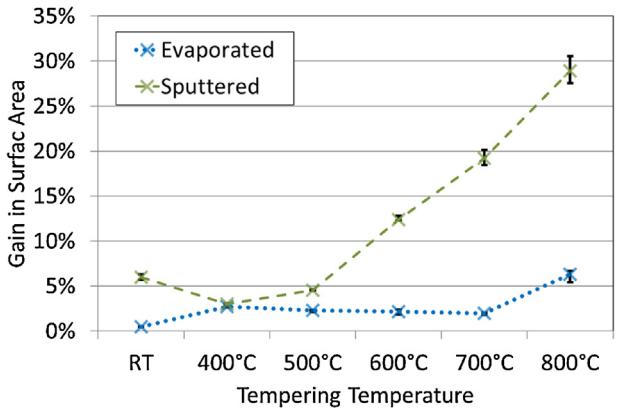

Fig. 9. AFM statistical evaluation of gain in surface area compared to an ideally flat one.

good that even the fine structure on top of grains is visible. Second, both thin film types have a closed surface. And finally, SEM cross-section imaging confirmed that the depth of valleys was not deeper than visible in AFM. From the AFM surface images in Fig. 8, it is apparent that the evaporated thin films are much smoother than the sputtered thin films. This holds also for the untempered thin films, which are compared in Fig. 9.

Fig. 9 shows the calculated gain in surface area by surface structure compared to an ideally flat surface, i.e. the bare substrate dimensions. Surface area is one of the limiting factors in photocatalysis: the greater the amount of reactant able to adsorb to the catalyst's surface at any one time, the greater the number of reactions taking place [11], if enough charge carriers are provided of course. Because UV irradiation was performed with 4.77 mW/cm^2, light is no bottle neck in this case and transport of reactants and products are limiting factors, inducing a first order rate reaction for photocatalysis. Another advantage of a larger surface area is that more surface bound hydroxyl groups will be present, which increase photocatalytic efficiency [4].

Evaporated thin films are very smooth with a roughness of 1.14 nm (RMS), whereas sputtered thin films start with greater surface roughness of 3.42 nm (RMS). At all annealing temperatures, the evaporated thin films do not change much in roughness and therefore surface area remains basically constant. Sputtered layers exhibit a gain in surface area of 6% (evaporated +0.5%) at RT that stays roughly constant until 500 °C, and then shows a pronounced increase up to a gain of 29%.

Therefore, we suggest that the larger surface area of sputtered thin films is one of the reasons why they have higher photocatalytic efficiency than both, evaporated thin films at 600 °C 1 h TAT and all other tested tempering TATs at this temperature, until rutile formation begins to dominate. The strong influence of surface area even appears to outperform the effect of texture.

3.5. Thin film structure and crystallization

In Fig. 10, SEM pictures of the two thin film types tempered at the highest tested temperature are shown, both in top view and cross section. Both films were X-ray amorphous directly after deposition. They show completely different crystallization behavior. As already shown, evaporated thin films start with a very smooth surface (AFM) and not as dense as sputtered thin films (UV–vis, ellipsometry). Additionally, a columnar growth structure is observed in amorphous phase in both thin film types, just a bit finer in the evaporated case and a little bit more pronounced in the sputtered case. The columnar fine structure of the sputtered thin film in top view is around 7 nm in diameter.

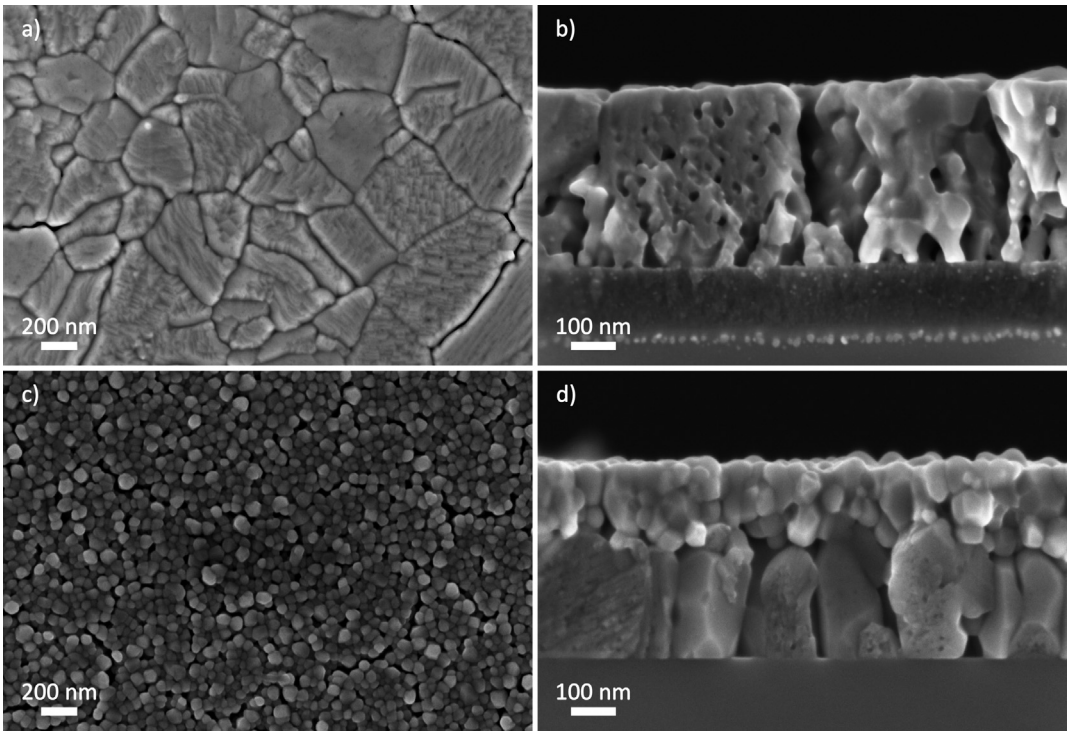

Fig. 10. SEM of both thin film types after tempering at 800 °C with TAT 1 h: (a) evaporated top view, (b) evaporated cross section, (c) sputtered top view, (d) sputtered cross section.

We will now focus on the nucleation and growth mechanism of the evaporated thin films. The evaporated thin films are deposited at room temperature and incoming TiO_x molecules only have energy on the order of k_BT. Consequently, thin film formation is far away from the melting temperature of TiO_2 and thermodynamic equilibrium. This causes a low nucleation barrier, leading to homogeneous nucleation. The high driving force to form crystallites leads to classical nucleation and grain growth everywhere in the bulk. In the SEM measurements of the corresponding temperature series, this is nicely visible. At 400 °C, very small grains in the range of a few nm are formed throughout the bulk. At higher temperatures, they grow bigger and are very similar in size. Instead of Ostwald ripening, they join upon touching to form bigger grains, possible because of their same size and therefore same chemical potential. This is similar to sintering. In this joining process, voids are left within the newly formed grains. They lead to porosity throughout each grain, and by this, throughout the whole thin film. During further reconstruction at even higher temperatures, the voids get bigger and their number is reduced. The driving force for reconstruction of these voids is attributed to reduction of surface area. At 800 °C, as shown in Fig. 10, grains are of about 200–600 nm in lateral size and reach the height of the complete film thickness. Summing up, the evaporated thin films underwent homogeneous nucleation, grain growth comparable to sintering, reconstruction of voids inside grains and they grew grains on the order of the film thickness.

In this paragraph, we will discuss the absence of rutile in evaporated thin films. Being far from thermodynamic equilibrium during deposition, it is unfavorable to form rutile nuclei at this stage. Due to homogeneous nucleation while tempering, anatase phase can form without problem, because rutile has a higher nucleation barrier. The astonishing stability of anatase, even up to 800 °C for 1 h TAT, could perhaps be explained by the special void formation inside the grains. Due to such voids, the actual surface area of each grain is much larger than that of a dense one. The cross section SEM images of the temperature series show that at 600 °C, there are a lot of very small voids in the grains. At 700 °C and 800 °C, grains are reconstructed more and more to decrease surface area and combine the many small voids to fewer, larger ones. Because anatase has lower surface energy than rutile [4,33,34], it is more favorable to have anatase at high surface to volume fractions. This seems to be the driving force here, that the anatase grains first reconstruct themselves to get a lower surface to volume fraction, before they can transform into the thermodynamically stable rutile phase.

Now we will focus on the nucleation and growth mechanism of the sputtered thin films. During sputter deposition, the growing thin film is heated due to transfer of kinetic energy of incoming atoms and ions to the film. The estimated temperature on top of the sample is roughly 200 °C shortly after starting deposition. Because of this, the film is significantly closer to its melting temperature and thermodynamic equilibrium during formation, compared to the evaporated thin films discussed earlier. One effect of this, shown before in ellipsometry results, is the higher refractive index already in amorphous state before tempering. This indicates a denser thin film. The driving force of forming nuclei is so low that they do not form randomly in bulk, but instead need a nucleation site at a layer interface. In this case, an interface is given by the border of TiO_2–SiO_2. This induces heterogeneous nucleation, as seen in SEM cross section of the temperature series of sputtered thin films. Nuclei form at this interface and start to grow from there upwards throughout the thin film. The TiO_2 thin film is divided by this mechanism into two distinct layers as shown in Fig. 10. At lower temperatures, including 500 °C, the main crystallized part of the sputtered thin film is buried underneath a nearly amorphous layer. This may likely explain the comparatively low photocatalytic efficiency observed for sputtered thin films tempered at 400 °C and 500 °C. At higher temperatures, the nucleation barrier can be overcome also in the upper residual amorphous layer. Grain growth and Ostwald ripening inside the top layer is visible in the top view SEM pictures for 600 °C and higher. There are only significant number of anatase grains at the surface of the sputtered thin films after annealing at 600 °C. Thus, it makes sense that at this temperature

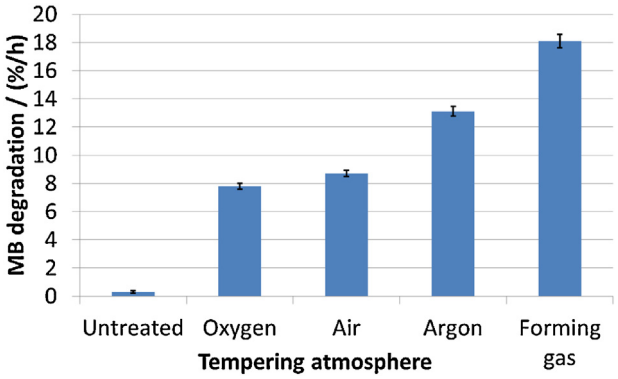

Fig. 11. Methylene blue degradation efficiencies of evaporated TiO_2 thin films, tempered at 600 °C for 1 h at different atmospheres. The "untreated" film is not tempered for comparison.

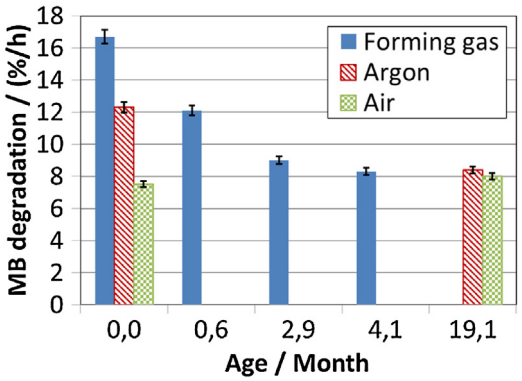

Fig. 12. Evaporated TiO_2 thin films tempered under different atmospheres. Repeated methylene blue degradation test over a period of several months.

there is a big efficiency increase as discussed earlier. It is shown in literature that it is especially important to have the anatase phase at the interface to the solution [4,7].

In this last paragraph of the crystallization section, we will discuss the formation of rutile in sputtered thin films. Nucleation of rutile, being the thermodynamically stable phase of TiO_2, is promoted by the higher deposition temperature during sputtering compared to evaporation. For small grain sizes at low temperatures, grain growth of existing anatase nuclei is favored above grain growth of existing rutile nuclei, as discussed in the second last passage about rutile formation in evaporated layers. Initial rutile nuclei up to a diameter of about 2 nm are not expected to be seen in XRD, because of very low volume fraction on the one hand, and small grains combined with no existing material contrast on the other. Considering these three aspects, we suggest that small rutile nuclei were already formed during sputter deposition, but did not grow at lower temperatures. Only starting from 600 °C, the growth barrier is low enough that both phases undergo grain growth.

3.6. *Tempering atmospheres, oxygen vacancy defects and thin film aging*

Lastly, we will discuss the effect on photocatalytic efficiency of different atmospheres during tempering, the positive effect of oxygen vacancy defects and aging of these thin films. There has been an increase of attention in research recently for the influence of oxygen vacancy defects on the photocatalysis of TiO_2 [35]. There are mainly two scopes of application for inducing oxygen vacancies. One is to shift light absorption to the visible regime without the necessity of dopants, promoting the usage for sunlight applications [16]. This strategy might be very promising for water purification in developing countries. The other one is to alter the electronic state at the surface, promoting the chemical reactions during photocatalysis [36]. The requirements of both applications are different. For the former, it is important to have a shift in band gap energy and good absorption of visible light in the entire bulk. Thus, oxygen vacancy defects are needed throughout the bulk. But for the latter, i.e. surface optimization for UV-light applications, bulk defects are unfavorable because they also act as trap states and charge carrier recombination centers, reducing the amount of available charge carriers at the surface [16]. Hence, only oxygen vacancy defects at the surface are desirable. The focus of our experiment is on oxygen vacancy defects at the surface to improve photocatalytic efficiency under UV irradiation.

It has been reported that rutile formation could be promoted by a reducing atmosphere, i.e. because defect sites promote rutile formation [33]. XRD measurements however show no indication of rutile in this atmosphere series at 600 °C with 1 h TAT. The main difference in the chosen atmospheres is their effect in measures of being oxidizing or reducing, ordered in Fig. 11 accordingly. Argon, an inert gas, is not reducing. But used as a pure and inert atmosphere, it hinders oxygen from reaching the thin film during tempering. As deposited, the thin films are expected to be a bit sub-stoichiometric. Therefore, the thin films tempered in argon atmosphere are expected to be sub-stoichiometric after tempering, too. Forming gas ($N_2 + H_2$) can even be expected to induce a significant number of oxygen vacancies, leading to the most pronounced sub-stoichiometry thin films in this series. Because the evaporated thin films are alike after deposition and rutile is absent after tempering, and the atmospheres only alter the amount of oxygen vacancies, the following discussion will focus on the latter.

In Fig. 11 the methylene blue degradation efficiencies of evaporated TiO_2 thin films tempered at 600 °C for 1 h at different atmospheres show significant differences, as expected. The thin film tempered in pure oxygen can be taken as the one which has annealed out the most with respect to oxygen vacancy defects, i.e., being as close as possible to stoichiometry given the structural confinements. Air consists of enough oxygen to anneal out defects, too. As expected it is very close to the efficiency of the oxygen treated thin film. The slight difference can possibly be due to the humidity of air compared to pure oxygen gas. Attaching OH-groups at the surface may hinder the healing process. The significantly best thin film is the one tempered in forming gas, having more than twice the photocatalytic efficiency than the standard one tempered in air. By itself this is an outstanding improvement and would be great to have for applications. However, our aging measurements show a continuous decline in effect, which will now be discussed.

Because oxygen treated samples are so similar to the ones tempered in air, they are left out of this comparison. In Fig. 12, repeated measurements of methylene blue degradation are shown over a period of 19 months. The thin film tempered in air atmosphere remained stable for the full period with regard to its photocatalytic efficiency. The others, thin films treated in argon and forming gas, show a decrease in efficiency over time, reaching exactly the same efficiency of the air-treated thin films. As shown for forming gas, the efficiency decline is not abrupt, but exponential with saturation at the lower limit of the efficiency of the thin film tempered in air. This indicates that the induced oxygen vacancy defects are annealed out over time and therefore are considered to be a case of sample aging. At first it was suspected that the methylene blue degradation measurement could have induced the aging. That is why comparative measurements were made in addition with thin films of the same batch, which were not measured with methylene blue until then. It turned out that they showed the same aging effect.

This shows that reduced TiO_2 thin films with surface oxygen vacancy defects that are stored in normal atmosphere at room temperature are subject to aging in the sense of efficiency decline. It is not a short term effect, but already after 3 months, the gain in efficiency is negligible, taking into account the extra effort in production. Considering the initial large gain in efficiency, further research could address this interesting aging problem.

There has been a report, that oxygen defects could have been stabilized in the bulk, if surrounded by a shell of stoichiometric TiO_2 (tested for one year) [13]. But this strategy is only useful for the purpose of shifting the light absorption to the regime of visible light as outlined in the beginning of this section. It is therefore not feasible in this case, where surface defects are necessary. A possible workaround for applications could be to store the reduced thin films under vacuum until needed. In addition, it could be feasible to have a service interval of 3 months, at which time they are tempered again in forming gas. A permanent solution would be, of course, highly favorable and should be subject of further research.

4. Conclusion

The present study reveals significant differences in the crystallization behavior and resulting properties of evaporated versus sputter deposited titania thin films. While evaporated thin films followed the path of homogeneous nucleation and grain growth, sputtered thin films were subject to heterogeneous nucleation. The latter lead to grains growing from bottom to top initiated by the SiO_2 interface, creating a two layer system up to 800 °C with 1 h TAT. Therefore, the good crystallinity of sputtered thin films was buried underneath a top layer which stayed nearly amorphous up to 500 °C. Starting from 600 °C, the temperature was high enough to induce significant grain growth also in the top layer. As a result, the photocatalytic efficiency of sputtered thin films increased significantly starting from 600 °C, whereas evaporated thin films showed a continuous increase over the full temperature regime.

Analysis of surface structure revealed that the evaporated thin films stayed very smooth over the full temperature regime of tempering, leading to no significant gain in surface area. An increase in surface area would promote the amount of adsorbing reactants and therefore raise photocatalytic efficiency, assuming enough charge carriers are provided at the reaction sites. In contrast to evaporated thin films, sputtered thin films showed a continuous increase in surface area up to a gain of about 30% over increasing tempering temperatures. This increase in surface area in sputtered thin films is considered to be the reason why sputtered thin films performed better than evaporated thin films after tempering at 600 °C for 1 h.

The further increase in surface area of sputtered thin films at even higher temperatures could, however, not compensate for the disadvantageous rutile formation. Rutile, known to be mainly counterproductive for photocatalysis, did not occur for evaporated layers up to 800 °C with 1 h TAT, whereas it started to be measurable for sputtered layers already after tempering at 600 °C with 1 h TAT.

Surface oxygen vacancy defects are a very promising way to increase photocatalytic efficiency of TiO_2 thin films. This was shown exemplarily for tempering in reducing atmospheres. With tempering in forming gas, more than twice the photocatalytic efficiency was observed compared to tempering in air. It is unfortunate for applications that the induced oxygen vacancy defects are healing out when stored under normal conditions. After a period of 4 months their efficiency reached the lower limit of standard thin films tempered in air. Due to the high gain in efficiency, it seems worthwhile to find solutions to this aging problem with further research. At the present stage, however, all concepts based on the application of surface oxygen vacancy defects to improve photocatalytic efficiency have to be treated with caution regarding aging effects. For application purposes, aging tests are highly advisable.

Acknowledgements

This project was funded by the German Federal Ministry of Education and Research (BMBF) via project “Nanopurification” #03X0083E. C. Lamprecht acknowledges support by EC grant International European Fellowships PIEF-GA-2012-330418 – Graphite4Med. The authors thank Christoph Ochmann and Stefan Rehders for their technical assistance. The authors thank Brook Shurtleff for proofreading the final text.

References

[1] C.F. Goodeve, J.A. Kitchener, The mechanism of photosensitisation by solids, Trans. Faraday Soc. 34 (1938) 902, http://dx.doi.org/10.1039/tf9383400902
[2] A. Fujishima, K. Honda, Electrochemical photolysis of water at a semiconductor electrode, Nature 238 (1972) 37–38, http://dx.doi.org/10.1038/238037a0
[3] H. Ibach, H. Lüth. Solid-state physics: an introduction to principles of materials science. 2010, doi: 10.1007/978-3-540-93804-0.
[4] O. Carp, Photoinduced reactivity of titanium dioxide, Prog. Solid State Chem. 32 (2004) 33–177, http://dx.doi.org/10.1016/j.progsolidstchem.2004.08.001
[5] T. Luttrell, S. Halpegamage, J. Tao, A. Kramer, E. Sutter, M. Batzill, Why is anatase a better photocatalyst than rutile? Model studies on epitaxial TiO_2 films, Sci. Rep. 4 (2014) 4043, http://dx.doi.org/10.1038/srep04043
[6] A. Kafizas, C.J. Carmalt, I.P. Parkin, Does a photocatalytic synergy in an anatase-rutile TiO_2 composite thin-film exist? Chemistry 18 (2012) 13048–13058, http://dx.doi.org/10.1002/chem.201201859
[7] R. Marschall, Semiconductor composites: strategies for enhancing charge carrier separation to improve photocatalytic activity, Adv. Funct. Mater. 24 (2014) 2421–2440, http://dx.doi.org/10.1002/adfm.201303214
[8] R. Su, R. Bechstein, L. Sø, R.T. Vang, M. Sillassen, B. Esbjörnsson, et al., How the anatase-to-rutile ratio influences the photoreactivity of TiO_2, J. Phys. Chem. C 115 (2011) 24287–24292, http://dx.doi.org/10.1021/jp2086768
[9] M. Kaneko, I. Okura. Photocatalysis: Science and Technology, Springer, 2002. http://www.amazon.de/Photocatalysis-Technology-Biological-Biomedical-Engineering/dp/3540434739/ (accessed 06.26.14).
[10] M.R. Hoffmann, S.T. Martin, W. Choi, D.W. Bahnemannt, Environmental applications of semiconductor photocatalysis, Society (1995) 69–96.
[11] A.M. Luís, M.C. Neves, M.H. Mendonça, O.C. Monteiro, Influence of calcination parameters on the TiO_2 photocatalytic properties, Mater. Chem. Phys. 125 (2011) 20–25, http://dx.doi.org/10.1016/j.matchemphys.2010.08.019
[12] V.I. Shapovalov, Nanopowders and films of titanium oxide for photocatalysis: a review, Glass Phys. Chem. 36 (2010) 121–157, http://dx.doi.org/10.1134/S108765961002001X
[13] Q. Zhu, Y. Peng, L. Lin, C.-M. Fan, G.-Q. Gao, R.-X. Wang, et al., Stable blue $TiO2_x$ nanoparticles for efficient visible light photocatalysts, J. Mater. Chem. A 2 (2014) 4429, http://dx.doi.org/10.1039/c3ta14484d
[14] X. Jiang, Y. Zhang, J. Jiang, Y. Rong, Y. Wang, Y. Wu, et al., Characterization of oxygen vacancy associates within hydrogenated TiO_2: a positron annihilation study, J. Phys. Chem. C 116 (2012) 22619–22624, http://dx.doi.org/10.1021/jp307573c
[15] T.L. Thompson, J.T. Yates, Surface science studies of the photoactivation of TiO_2 – new photochemical processes, Chem. Rev. 106 (2006) 4428–4453, http://dx.doi.org/10.1021/cr050172k
[16] T. Leshuk, R. Parviz, P. Everett, H. Krishnakumar, R.A. Varin, F. Gu, Photocatalytic activity of hydrogenated TiO_2, ACS Appl. Mater. Interf. 5 (2013) 1892–1895, http://dx.doi.org/10.1021/am302903n
[17] K. Hashimoto, H. Irie, A. Fujishima, TiO_2 photocatalysis: a historical overview and future prospects, Jpn. J. Appl. Phys. 44 (2005) 8269–8285, http://dx.doi.org/10.1143/JJAP.44.8269
[18] S.M. Gupta, M. Tripathi, A review of TiO_2 nanoparticles, Chinese Sci. Bull. 56 (2011) 1639–1657, http://dx.doi.org/10.1007/s11434-011-4476-1
[19] L. Liu, Understanding the reaction mechanism of photocatalytic reduction of CO_2 with H_2O on TiO_2-based photocatalysts: a review, Aerosol Air Qual. Res. 2 (2014) 453–469, http://dx.doi.org/10.4209/aaqr.2013.06.0186
[20] X. Chen, S.S. Mao, Titanium dioxide nanomaterials: synthesis, properties, modifications, and applications, Chem. Rev. 107 (2007) 2891–2959, http://dx.doi.org/10.1021/cr0500535
[21] P.Y. Yu, M. Cardona, Fundamentals of Semiconductors, Springer Berlin Heidelberg, Berlin, Heidelberg, 2010, http://dx.doi.org/10.1007/978-3-642-00710-1
[22] K. Seeger. Semiconductor Physics: An Introduction, 8th ed., Springer, Berlin, Heidelberg, 2002. http://www.amazon.de/Semiconductor-Physics-Introduction-Advanced-Texts/dp/3540219579/ (accessed 08.12.14).
[23] International Organization for Standardization, ISO 10678–Fine ceramics (advanced ceramics, advanced technical ceramics)–Determination of photocatalytic activity of surfaces in an aqueous medium by degradation of methylene blue, Switzerland, 2010.

[24] DIN Deutsches Institut für Normung e.V., DIN 52980–Photocatalytic activity of surfaces–Determination of photocatalytic activity by degradation of methylene blue, 2008.
[25] A. Gribb, J. Banfield. Particle size effects on transformation kinetics and phase stability in nanocrystalline TiO_2, Am. Mineral. 82, (1997) 717–728. http://minsocam.org/MSA/AmMin/TOC/Articles_Free/1997/Gribb_p717-728_97.pdf (accessed 05.06.14).
[26] K.-N.P. Kumar, D.J. Fray, J. Nair, F. Mizukami, T. Okubo, Enhanced anatase-to-rutile phase transformation without exaggerated particle growth in nanostructured titania–tin oxide composites, Scr. Mater. 57 (2007) 771–774, http://dx.doi.org/10.1016/j.scriptamat.2007.06.039
[27] N. Roy, Y. Sohn, D. Pradhan, Synergy of low-energy {1 0 1} and high-energy {0 0 1} TiO_2 crystal facets for enhanced photocatalysis, ACS Nano 7 (2013) 2532–2540, http://dx.doi.org/10.1021/nn305877v
[28] H.G. Yang, C.H. Sun, S.Z. Qiao, J. Zou, G. Liu, S.C. Smith, et al., Anatase TiO_2 single crystals with a large percentage of reactive facets, Nature 453 (2008) 638–641, http://dx.doi.org/10.1038/nature06964
[29] A. Selloni, Crystal growth: anatase shows its reactive side, Nat. Mater. 7 (2008) 613–615, http://dx.doi.org/10.1038/nmat2241
[30] J. Zhang, W. Chen, J. Xi, Z. Ji, {0 0 1} Facets of anatase TiO_2 show high photocatalytic selectivity, Mater. Lett. 79 (2012) 259–262, http://dx.doi.org/10.1016/j.matlet.2012.04.045
[31] L. Ye, J. Mao, J. Liu, Z. Jiang, T. Peng, L. Zan, Synthesis of anatase TiO_2 nanocrystals with {1 0 1} {0 0 1} or {0 1 0} single facets of 90% level exposure and liquid-phase photocatalytic reduction and oxidation activity orders, J. Mater. Chem. A 1 (2013) 10532, http://dx.doi.org/10.1039/c3ta11791j
[32] J.L. Giocondi, P.a. Salvador, G.S. Rohrer, The origin of photochemical anisotropy in $SrTiO_3$, Top. Catal. 44 (2007) 529–533, http://dx.doi.org/10.1007/s11244-006-0101-y
[33] D.a.H. Hanaor, C.C. Sorrell, Review of the anatase to rutile phase transformation, J. Mater. Sci. 46 (2010) 855–874, http://dx.doi.org/10.1007/s10853-010-5113-0
[34] U. Diebold, The surface science of titanium dioxide, Surf. Sci. Rep. 48 (2003) 53–229, http://dx.doi.org/10.1016/S0167-5729(02)00100-0
[35] X. Pan, M.-Q. Yang, X. Fu, N. Zhang, Y.-J. Xu, Defective TiO_2 with oxygen vacancies: synthesis properties and photocatalytic applications, Nanoscale 5 (2013) 3601–3614, http://dx.doi.org/10.1039/c3nr00476g
[36] X. Yu, B. Kim, Y.K. Kim, Highly enhanced photoactivity of anatase TiO_2 nanocrystals by controlled hydrogenation-induced surface defects, ACS Catal. 3 (2013) 2479–2486, http://dx.doi.org/10.1021/cs4005776.